

Clusters under strong VUV pulses: A quantum-classical hybrid-description incorporating plasma effects

Ionuț Georgescu, Ulf Saalmann and Jan M. Rost
Max Planck Institute for the Physics of Complex Systems
Nöthnitzer Straße 38, 01187 Dresden, Germany

(Dated: October 30, 2018)

The quantum-classical hybrid-description of rare-gas clusters interacting with intense light pulses which we have developed is described in detail. Much emphasis is put on the treatment of screening electrons in the cluster which set the time scale for the evolution of the system and form the link between electrons strongly bound to ions and quasi-free plasma electrons in the cluster. As an example we discuss the dynamics of an Ar_{147} cluster exposed to a short VUV laser pulse of 20 eV photon energy.

PACS numbers: 36.40.Gk, 32.80.-t, 52.50.Jm, 36.40.Wa

I. INTRODUCTION

The interaction of rare-gas clusters with intense laser pulses has attracted considerable attention over the last decade since spectacular experiments showed how effective energy from the laser beam can be coupled into the cluster, culminating in the demonstration of fusion in exploding deuterium clusters [1]. Other efforts aim at understanding the interaction of matter beyond a few atoms with light of different wavelength, motivated by the fact that little is known about such processes with intense light of frequencies different than the infrared (IR) range around 800 nm wavelength. First experiments at FLASH in Hamburg have revealed very efficient energy absorption at 98 nm wavelength [2] and have triggered theoretical research [3, 4, 5, 6] as recently reviewed [7].

Clearly, the time-dependent description of a finite many-body system interacting with a laser pulse is challenging. A full quantum description is numerically impossible and would probably provide little insight conceptually. One can observe two different strategies in the literature to tackle this problem: (i) A more or less full quantum approach for a single atom in the cluster treating the influence of the other atoms and ions in the cluster more approximately as a kind of environment [3, 8]. (ii) A classical propagation of all charged particles in time (ions and electrons) with quantum mechanical elements added in form of rates on various levels of sophistication [9, 10, 11, 12, 13, 14, 15, 16].

We have followed the latter route, describing the motion of all charged particles classically, while they interact and are subjected to the external dipole-coupled laser field. Initial bound electronic motion is not treated explicitly, but only in form of (quantum) ionization rates which are integrated into the classical dynamics with a Monte Carlo scheme, see [7]. The approach works very well, as long as the electrons, once ionized from their mother-ions, behave essentially classically. This is the case if they are subject to a strong external field (as it is the case with strong IR pulses) or are instantaneously free (as in the case of hard X-rays). Under VUV radi-

ation, however, the photo-electrons stay often very close to their mother-ions or other ions, effectively screening them and modifying subsequent ionization processes.

The reason for this behavior is the size of the quiver motion (typically less than a ground state electron orbit of the rare-gas atom) and the small kinetic energy which remains of the photon energy in excess of the ionization potential. The latter is not the case for hard X-rays where the photon energy is high enough to remove the photo-electrons completely from the cluster (at least for moderate cluster sizes). For intense IR-fields, on the other hand, the photon energy is much too low for the photo-electrons to leave the cluster instantaneously, but the quiver motion is (for typical intensities) of the size of the cluster or even larger implying that the photo-electrons certainly will not remain in the vicinity of specific ions. Rather, they are dragged back and forth through the cluster by the laser field. Hence, the photo-ionization of ions surrounded by screening electrons is a phenomenon unique to VUV radiation, adding to the challenge for a theoretical description. On the other hand, as will become clear subsequently, exactly those electrons which screen individual ions define a timescale, suitable to formulate a coarse grained electron dynamics in the cluster. It is the key to incorporate physical processes which in our approach lie at the interface of classical and quantum description, such as the influence of the surrounding charged particles (ions and electrons) on the photo-ionization rate of an ion in the cluster.

In the next section we summarize our quantum-classical hybrid description which contains the quantum photo-ionization rates of multi-electron ions, the classical propagation, and, as an element in between, the treatment and identification of those electrons which screen the ions. In Sect. III we explain how to deal with photo-ionization of bound electrons into the plasma of cluster electrons. Section IV discusses as an application and illustrative example the illumination of Ar_{147} with a VUV pulse of 62 nm wavelength. The paper ends with a short summary in Sect. V.

II. HYBRID-DESCRIPTION OF TIME-DEPENDENT CLUSTER EVOLUTION

The interaction of a cluster with intense radiation can be partitioned into three parts: (A) atomic ionization, (B) cooperative interaction of ions among each other and with electrons, and (C) relaxation. During phase (A) which lasts approximately until every second atom in the cluster is (singly) ionized, one can simply apply the atomic photo ionization cross sections for many-electron atoms supplied, e.g., in [17, 18]. Gradually, the bound electrons feel the cluster environment, which has roughly three effects (i) the ionization potential is lowered through close by ions, (ii) previously ionized electrons trapped by the cluster screen the ion under consideration, (iii) the global field, generated by electrons and ions, modifies the ionization potential as well. We will treat all three effects which happen during phase (B) of the dynamics in Sect. III. Here, we describe briefly how to extrapolate the known photo-ionization cross sections below the ionization threshold.

A. Atomic photo-ionization

The calculation of photo-ionization and excitation for individual energy levels of isolated atoms and ions is straight forward. Including the (quantum) photo rates into the classical propagation of charged particles in the cluster, we do not resolve the angular dependences of the photo cross section. Averaging over angular degrees of freedom considerably simplifies the cross sections which only depend on the radial wavefunctions for the respective mean initial and final energies of the photo transition, for a similar philosophy see [6]. We start from the dipole matrix element for linearly polarized light along the \hat{z} direction and consider the transition between initial and final atomic states with well defined orbital quantum numbers lm

$$\langle f|z|i\rangle = d_r(\ell_f, \ell_i) \int d\Omega Y_{\ell_f m_f}^*(\Omega) \cos\theta Y_{\ell_i m_i}(\Omega) \quad (1)$$

with the radial dipole matrix element

$$d_r(\ell_i, \ell_f) = \int_0^\infty dr u_{\ell_f}(r) r u_{\ell_i}(r). \quad (2)$$

Within the independent particle picture all states in a shell defined by orbital angular momentum ℓ_i are degenerate and have the same radial wavefunction $u_{\ell_i}(r)$. It is an eigenfunction to a spherically symmetric effective single particle potential obtained (along with the eigenfunction) from the Cowan code [17]. Within this mean field approximation the full photo cross section is easily obtained by summing over all available final states and averaging over the initial states in the shell ℓ ,

$$\sigma_\ell(\omega) = \frac{w_i}{3} \frac{4\pi^2\alpha\omega}{2\ell+1} [(\ell+1)d_r^2(\ell, \ell+1) + \ell d_r^2(\ell, \ell-1)]. \quad (3)$$

Here, w_i gives the number of available initial electrons.

Furthermore, in the cluster the ions are surrounded by other electrons and ions. The latter lower the potential barriers for ionization into the cluster. Hence, what is discrete photo excitation in an isolated atom becomes at the same photon energy ionization into the cluster. Therefore, we need an interpolation of the discrete excitation spectrum distributing the oscillator strength over the respective photon energy interval.

In the following, we compare two different interpolations. The first one is taken from [19]. There, approximate analytical expressions for the photo-absorption of many electron atoms are derived. The corresponding results for the Ar atom are shown in Fig. 1 with dashed lines. For comparison, the cross sections with hydrogenic wavefunctions [20] are also shown. In the second approximation we define a continuous photo-absorption in the region of discrete spectral lines by demanding that the renormalized photo excitation cross section merges smoothly with the photo-ionization cross section at threshold [21]. This is achieved by distributing the the oscillator strength f_n of a spectral line E_n over an interval half way to each of the adjacent lines such that

$$\sigma_n(\omega) = \frac{2\pi\alpha f_n}{(E_{n+1} - E_{n-1})/2}, \quad (4)$$

where $\sigma_n(\omega)$ is now the interpolated photo-absorption cross section Eq. (3) for $(E_{n-1} + E_n)/2 < \omega < (E_n + E_{n+1})/2$. The result (solid line in Fig. 1) shows reasonable agreement with the analytical approximation for low and high energies. For intermediate energies, the well known Cooper minima lead to considerably lower values than in the analytical approximation which does not account for this interference effect. Hence, we will use in the following the approximation Eq. (4).

B. Classical propagation for the Coulomb interaction under VUV radiation

The propagation of the classical particles is in principle straight forward. More refined methods, such as tree-codes are only worth the effort of coding for large clusters (10^5 electrons and ions and more). Another issue is the Coulomb interaction. Using the real Coulomb potential with its singularity is numerically very costly (small time steps close to the singularity) and leads for more than two bound electrons to artificial autoionization since one electron can fall into the nucleus (below the quantum ground state energy) and another one can be ionized with the released energy. In strong field physics (at IR frequencies) the so called soft-core potential

$$U(r) = -\frac{Z}{(r^2 + a^2)^{1/2}} \quad (5)$$

has been used routinely where the singularity is cut off by the smoothing parameter a chosen to get potential depths (slightly) below the true ionization potential

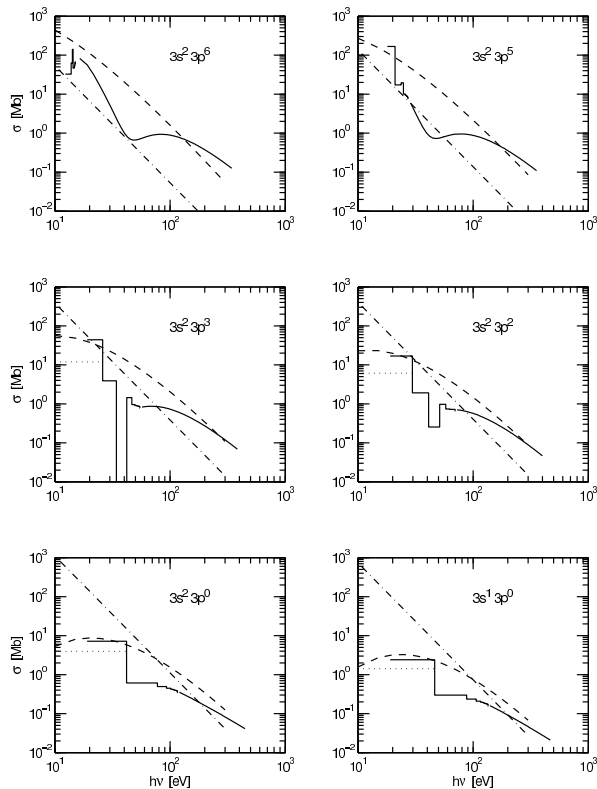


FIG. 1: Atomic photo-ionization rates extrapolated below the threshold according to [19] (dashed) and by interpolation of the discrete spectrum (solid). The dashed-dotted line is an approximation with hydrogenic wavefunctions, see text. The initial configuration is displayed in each panel.

of the atom or ion. As long as the quiver amplitude $x_{\text{quiv}} = F/\omega^2 \gg a$, the cut off is irrelevant for the dynamics, as it is typically the case for a strong pulse (for $3 \times 10^{16} \text{W/cm}^2$ and 800 nm wavelength, $x_{\text{quiv}} \approx 500 a_0$ while a is of the order of $1 a_0$). However, at 10 times higher photon frequency and a factor 100 weaker peak intensity which is realistic, e.g., for the FLASH source in Hamburg, $x_{\text{quiv}} \approx a$. Even more problematic is the fact that the soft-core potential is harmonic about its minimum with a characteristic frequency $(Z/a^3)^{1/2}$ which could become resonant with the VUV laser frequency.

To avoid these problems we use a different approximate potential which has the correct asymptotic Coulomb behavior at large distances but lacks an eigenfrequency since it has a non-zero slope at $r = 0$,

$$V(r) = -\frac{Z}{r}(1 - e^{-r/a}). \quad (6)$$

Here, a is chosen in analogy to the potential (5) discussed above. Note that $U(r \rightarrow 0) = V(r \rightarrow 0) = -Z/a$. For rare-gas atoms a is of the order of one: $a = 1.74$ for Xe and $a = 1.4$ for Ar.

For the photon frequency used here ($\hbar\omega = 20 \text{ eV}$) there is no qualitative difference using a U-shape (soft-core) or a V-shape potential. The subsequent considerations also

do not depend on the approximate or exact form of the Coulomb potential. Therefore we will use the generic form $v(i, j)$, which could be either of the three options:

$$v(i, j) = \begin{cases} |\mathbf{r}_i - \mathbf{r}_j|^{-1} & \text{exact Coulomb} \\ [(\mathbf{r}_i - \mathbf{r}_j)^2 + a^2]^{-\frac{1}{2}} & \text{U-shape} \\ (1 - e^{-|\mathbf{r}_i - \mathbf{r}_j|/a}) |\mathbf{r}_i - \mathbf{r}_j|^{-1} & \text{V-shape} \end{cases} \quad (7)$$

Our numerical examples presented here have been obtained with the V-shape potential.

C. Identification of localized and delocalized electrons

At photon energies comparable or less than the ionization potential of a cluster ion ($\hbar\omega \leq 30 \text{ eV}$), most of the photo-electrons remain in the cluster, i.e., quasi-free electrons are produced. They thermalize quickly, i.e., form a plasma.

We have to determine which among these quasi-free electrons travel all over the cluster and visit many ions (delocalized quasi-free electrons) and which revolve about a single ion, that is, are effectively in excited states about an ion (localized quasi-free electrons). To do so, we record the revolution angle $\phi(t)$ of each classical electron about its closest ion as a function of time. If the electron j moves for two revolutions ($\phi_{j\alpha} = 4\pi$) about the same ion α we consider it as localized, and the period of its motion $T^{j\alpha}$ is then given by $2\pi = \phi_{j\alpha}(T^{j\alpha})$.

The average period $\bar{T}^{j\alpha}$ of all localized classical electrons sets the time scale for a coarse grained dynamics. This time scale changes slowly in real time t due to changes in number and energy of the localized electrons, see Fig. 2. With an initial guess for the first averaged period $T_0 = 1 \text{ fs}$, we update T after a time $t = T_i$ according to the general sequel

$$\bar{T}_{i+1} = \frac{T_i}{n} \sum_{\alpha=1}^N \sum_{j_\alpha=1}^{n_\alpha} \frac{2\pi}{\phi_{j_\alpha}(T_i)}, \quad (8)$$

where the actual time interval used is increased by the standard deviation σ_{i+1} of the mean, $T_{i+1} = \bar{T}_{i+1} + \sigma_{i+1}$.

The coarse graining of time through the time intervals T_i , whose length is defined by the localized electrons, plays a crucial role for the description of the entire cluster dynamics. It provides the natural time scale to interpolate between the explicit time-dependent dynamics of the classical electrons and the time-averaged rate description of the bound “quantum” electrons. Over an interval $t_0 < t < t_0 + T_i$ in time all processes involving quantum rates will be considered within a fixed cluster environment with properties averaged over the previous interval $[t_0 - T_{i-1}, t_0)$.

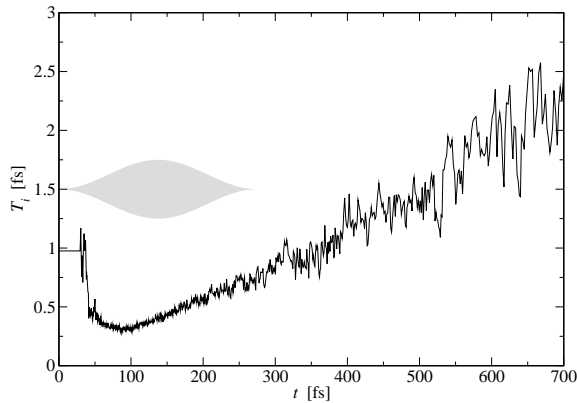


FIG. 2: Time intervals T_i of the averaged localized motion of the screening electrons as a function of real time for an Ar_{147} cluster with laser parameter as specified in Sect. IV.

III. COARSE GRAINED PHOTO-IONIZATION INTO THE PLASMA

We are now prepared to calculate atomic properties in the environment of other cluster ions and electrons with the understanding that all these processes are for a specific time interval T_i as introduced in the previous section. The photo-ionization dipole matrix elements for many-electron atoms provided within the Hartree-Fock approximation [17] allow one to determine the photo cross section for ionization of individual occupied orbitals to the continuum, see Sect. II A.

To apply these cross sections, we have to approximately map the present situation of a cluster ion surrounded by the localized electrons and other charged particles (ions and delocalized electrons) into an effective single ion scenario. This requires first to determine the electronic energy of an ion with its localized electrons and then to construct an energy-equivalent configuration.

A. Electronic energy of the ions including localized electrons

Averaged over T_i we calculate the number n_α of electrons localized about ion α and their mean energy

$$E_\alpha^* = E(q_\alpha) + \sum_{j=1}^{n_\alpha} \left(\frac{p_j^2}{2} - q_\alpha v(j, \alpha) \right) + \sum_{j>k=1}^{n_\alpha} v(j, k), \quad (9)$$

with $v(j, k)$, the interaction potential Eq. (7) between two particles of unit charge at positions \mathbf{r}_j and \mathbf{r}_k , q_α , the charge of the ion α and $E(q_\alpha)$ the energy of its bound electrons.

The localized electrons are in excited states of the ion α , as shown in Fig. 3. Starting from the energy E^* of this actual configuration, we include them in the photo-ionization process by constructing the equivalent configuration of ion α . In this configuration, we relax all local-

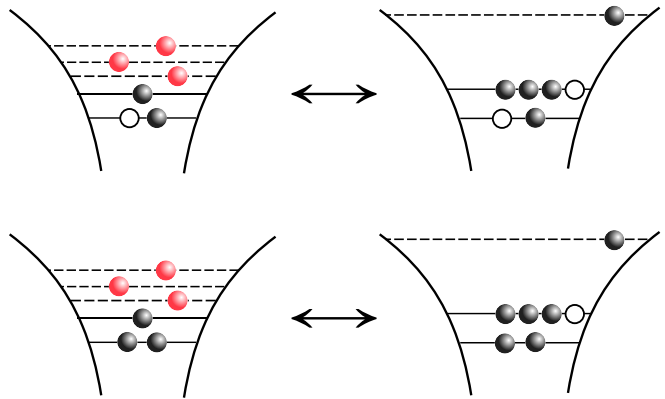


FIG. 3: Sketch for the construction of the equivalent electronic configuration (right panel) from the actual configuration (left panel) of a cluster ion with three localized electrons (red) around a $3s^1 3p^1$ (upper row) and $3s^2 3p^1$ (lower row) configuration. Holes are shown as open circles.

ized electrons but one onto the last occupied orbital of the actual configuration. We put the remaining electron on a Rydberg orbit, whose energy is given by the condition that the actual and the equivalent configuration have the same energy E^* .

B. Ionization potential of the equivalent configuration

To find the binding energy of electrons in occupied orbitals in the presence of a Rydberg electron, we assume that neither the quantum number n nor the angular momentum ℓ of the Rydberg electron change upon release of an electron from a deeper orbital. Then the ionization energy ΔE is given by

$$\Delta E(C_q, n) = E(C_{q+1}, n) - E(C_q, n), \quad (10)$$

where $E(C_q, n)$ is the energy of the valence shell configuration C with charge q and an additional electron in a Rydberg orbital n . We have omitted ℓ as an index in (10) since the following discussion does not depend on it. As an illustrative example we will use $\ell = 1$. The quantum number n can take values from n_0 up to ∞ , with n_0 corresponding to the situation where the ‘‘Rydberg’’ electron is in the lowest possible state; for Argon and $\ell = 1$ it is $n_0 = 3$. Figure 4 provides energies for six configurations and $n = 3 \dots 9$. In five of the configurations the valence shell does not contain electron holes. Thus they are solely defined by the charge: $C_q \equiv q$. The case $C'_2 = 3s3p^4np$, also shown in Fig. 4, is an example for an exception with a hole in $3s$. Obviously we have

$$E(C_q, \infty) = E(C_{q+1}, n_0) = E(C_q, n_0) + E_{\text{ip}}(C_q), \quad (11)$$

i. e. the asymptotic energy $n \rightarrow \infty$ of a Rydberg series coincides on one hand with the origin of the Rydberg series of the next higher charge state, as can be seen in

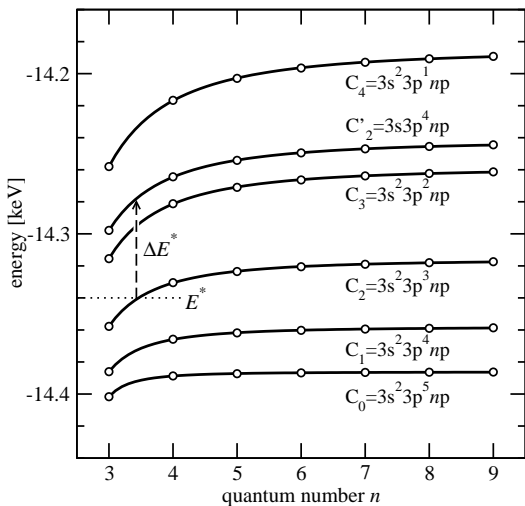


FIG. 4: Total energies (circles) for ions with one of the electrons in a Rydberg state with quantum number n and angular momentum $\ell = 1$. The valence shell configuration C_q is specified for each set of energies. Fitted curves (thick lines) according to Eq. (12). As an example the energy E^* for an equivalent configuration (dotted) as defined in Sect. III A and the corresponding energy ΔE^* for ionization (dashed) are shown.

Fig. 4. On the other hand it is equal to the sum of the ground-state energy and the ionization potential E_{ip} for an ion with configuration C_q . For finite values of n we approximate the energies by a quantum defect formula [22]

$$E(C_q, n) = E(C_q, \infty) - \frac{1}{2} \left(\frac{Z_{\text{eff}}}{n - \mu_q} \right)^2, \quad (12)$$

where in contrast to the usual ionic charge Z we use an effective one,

$$Z_{\text{eff}} = (n_0 - \mu_q) (2E(C_q, \infty) - 2E(C_q, n_0))^{1/2}, \quad (13)$$

chosen such that the first level (n_0) of the series agrees with the exact value while the quantum defect μ_q is fitted. Hence, Eq. (12) is very accurate at intermediate n , where we need it. When fitting the curves Eq. (12) to the calculated energies, cf. Fig. 4, we found the quantum defects μ_q to be almost independent of q . This allows us in the calculation of energy differences Eq. (10) to eliminate the term containing n and μ in Eq. (12). We get for a configuration C_q with an initial energy E^*

$$\Delta E^*(C_q) = [E(C_{q+1}, \infty) - E^*] - b [E(C_q, \infty) - E^*], \quad (14)$$

with

$$b := \frac{E_{\text{ip}}(C_{q+1})}{E_{\text{ip}}(C_q)}, \quad (15)$$

the ratio of the ionization potentials, cf. Eq. (11). Thus we have obtained an expression for the energy necessary to ionize an electron from a valence shell in presence of

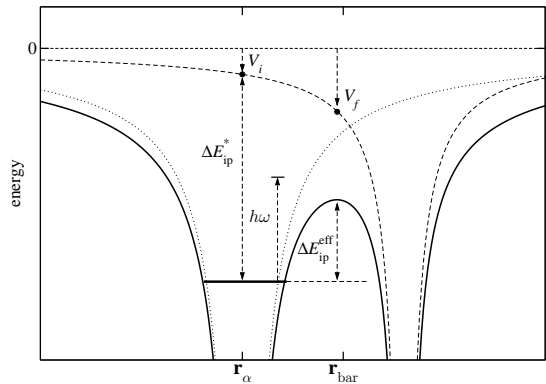


FIG. 5: Sketch of the energy balance for the photo-ionization of a cluster ion α . The cluster potential is represented by a single neighbouring ion. The thick full line indicates the full cluster potential, the thin long dashed line represents the cluster environment, i.e. the cluster potential without the contribution from the ion itself. The dotted line is the Coulomb potential for $q_\alpha + 1$, i.e. the field of the ion if the electron would be ionized. The interaction of the bound electron with the nucleus is represented by ΔE^* . The saddle point of $V(\mathbf{r}) - (q_\alpha + 1)v(\alpha, \mathbf{r})$ defines the position \mathbf{r}_{bar} of the barrier.

a Rydberg electron. This expression does not depend on the actual quantum numbers n and ℓ , but only on the energy E^* .

C. The condition for over-barrier inner-ionization

Although we know now with Eq. (14) the ionization potential for a screened isolated ion, we have to position the ion in the cluster environment in order to decide, if photo-absorption leads to photo-excitation within the ion α or to inner-ionization above the lowest barrier on the way to a neighbouring ion. The energy balance for the photo electron which decides between these two options is

$$E_i + V_i + \omega = E_f + V_f \quad (16)$$

with local contributions from the ion to which the electron is bound, (see Fig. 5)

$$E_i = -\Delta E^*, \quad E_f = E_{\text{kin}} - (q_\alpha + 1)v(\alpha, \text{bar}), \quad (17)$$

and contributions from the background of charges in the cluster,

$$V_i = -\sum_{j \neq \alpha} q_j v(j, \alpha), \quad V_f = -\sum_{j \neq \alpha} q_j v(j, \text{bar}), \quad (18)$$

where the index j runs over the delocalized electrons and all ions but ion α . As introduced earlier, $v(l, m)$ is the interaction between two Coulomb particles at positions \mathbf{r}_l and \mathbf{r}_m . Hence, V_i refers to the potential energy of the

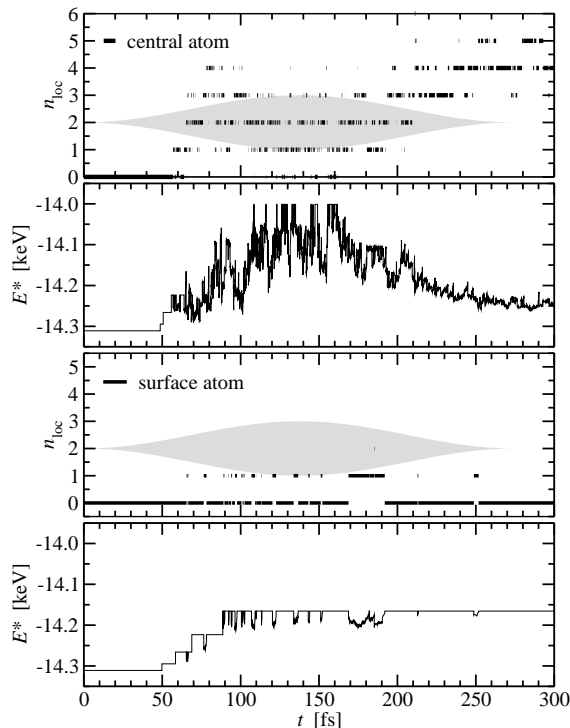


FIG. 6: The number of localized quasi-free electrons n_{loc} and the corresponding energy E^* according to Eq. (9) for the central ion and a surface ion of an Ar_{147} cluster from the microscopic calculation in Sect. IV.

electron under consideration and located at the position of its mother ion α due to interaction with particles of charge q_j at \mathbf{r}_j . Likewise, V_f is the potential energy of the same electron at the potential barrier \mathbf{r}_{bar} due to the interaction with the same charged particles as before. The energy balance Eq. (16) is taken with respect to the location of the ion \mathbf{r}_α and the location \mathbf{r}_{bar} of the lowest potential barrier near the ion. ΔE^{eff} in Fig. 5 is defined by putting $E_{kin} = 0$ in Eq. (17), i.e.,

$$\Delta E^{eff} = \Delta E^* - (q_\alpha + 1)v(\alpha, bar) + V_f - V_i. \quad (19)$$

Figures 6 and 7 give an overview of the coarse grained variables during the laser pulse for an atom at the center and one at the surface of the Ar_{147} cluster. Figure 6 shows first of all an overview of their evolution during the whole interaction with the laser. Starting at the ground state of the neutral Ar, each absorbed photon leads to a rising step in the total energy. Note that for an ion in the cluster the electron has to be excited only above the lowest barrier. Moreover, the energy E^* of the equivalent configuration takes merely the localized electrons into consideration and not the newly ionized one. Therefore, each ionization event leads to jumps of E^* higher than the energy of the photon, cf. Fig. 6.

The electron localization is equivalent to a relaxation of the system and lowers therefore E^* . The flat regions observable for both ions correspond to the case where there

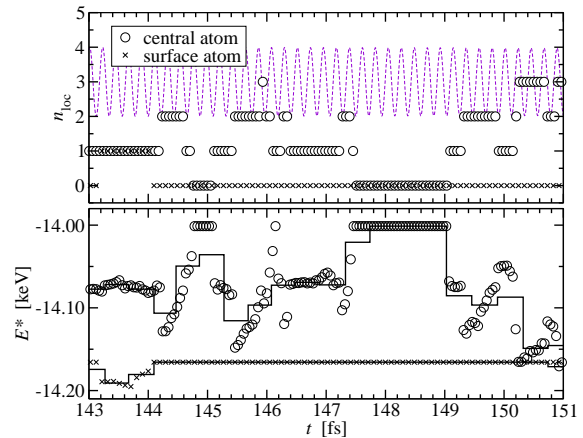


FIG. 7: Zoom into Fig. 6 for $143 < t < 151$ fs. The upper panel shows the number of localized electrons (\circ for the central atom, where $q = 6$ and \times for the surface atom, $q = 4$). The lower panel shows the total energy E^* of the ions and their localized electrons. The full lines show here the average of E^* over the time intervals T_i , as introduced in Section II C.

are no localized electrons, when the total energy of the ion is given solely by the bound, “quantum” electrons. The smaller final charge of the surface atom is a consequence of the cluster expansion. The surface expands much faster than the core, leading to higher interionic barriers and an early suppression of the inner-ionization. A detailed view of the evolution of the two atoms is shown in Fig. 7 for the time interval from $t = 143$ to 151 fs. The coarse graining is symbolized by the full lines, showing the total energy E_α^* of the two atoms averaged over the time intervals T_i , as described in Sect. II C.

D. The effective cross section for inner photo-ionization

Finally, we are in a position to adopt the photo-ionization cross section as formulated in Sect. IIA for an isolated ion to the situation of an ion in the cluster. Here, we take the lowest potential barrier to a neighboring ion as effective ionization threshold. Therefore, the actual cross section as shown in Fig. 1 can vary between minimum and maximum possible values of potential barriers. The interval is indicated for small photon energies in Fig. 1 with the additional dotted line.

The electrons available for photo-ionization are only the tightly bound ones from the actual configuration, while the matrix elements entering the expression for the cross section Eq. (3) take into account the screening of the electrons as provided by the equivalent configuration $\sigma = \sigma(q_{eqv})$. Hence, the multiplicity has to be taken from the actual configuration w_{act} to arrive at the screened photo cross section

$$\sigma^{scr}(q) = \frac{w_{act}}{w_{eqv}} \sigma(q_{eqv}). \quad (20)$$

IV. DYNAMICS OF Ar_{147} UNDER AN INTENSE VUV LASER PULSE

We will illustrate the theoretical framework introduced above with the dynamics of Ar_{147} exposed to a 100 fs VUV laser pulse with $\hbar\omega = 20$ eV (i.e. wavelength $\lambda = 62$ nm) and an intensity of 7×10^{13} W/cm². Figure 8 shows the main quantities characterizing the response of the cluster to the VUV pulse, namely the energy absorption, the ionization degree, the temperature of the plasma and the cluster explosion. The latter is characterized by the interionic distance R_{avg} , defined as

$$R_{\text{avg}} = \sqrt{\frac{1}{N} \sum_{\alpha=1}^N \min_{\beta \neq \alpha} (|\mathbf{r}_\beta - \mathbf{r}_\alpha|^2)}. \quad (21)$$

In the first part of the pulse, until approximately $t = 80$ fs, the absorption is dominated by photo-ionization. After that, inverse bremsstrahlung (IBS) sets in and photo-ionization starts to saturate. We can easily disen-

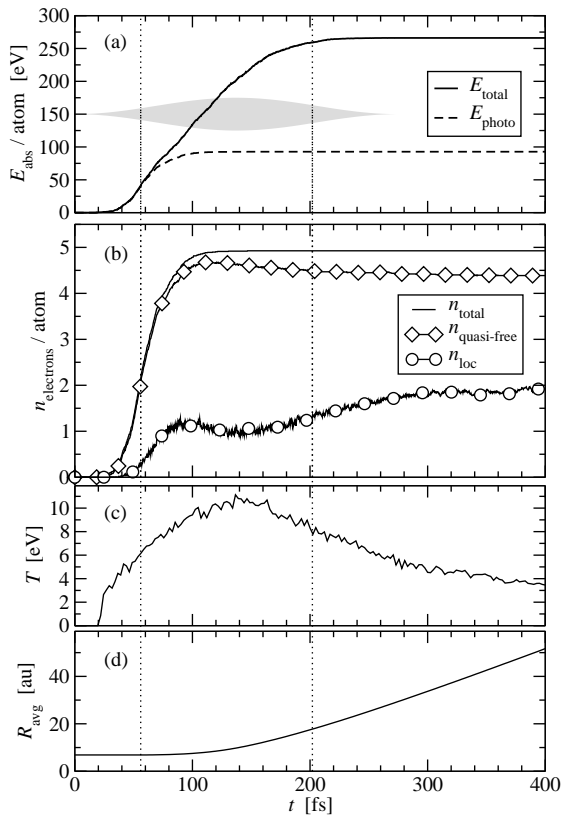


FIG. 8: Explosion of Ar_{147} exposed to a 100 fs long VUV laser pulse with intensity $I = 7 \times 10^{13}$ W/cm² and photon energy $\hbar\omega = 20$ eV. (a) full-line: total absorbed energy per atom; dashed-line: energy absorbed due to photo-ionization; (b) full-line: total number of ionized electrons per atom; \diamond quasi-free electrons; \circ localized electrons; (c) temperature of the quasi-free electrons; (d) expansion: average interionic distance, see Eq. (21).

tangle the two contributions to the total absorbed energy since we treat photo-ionization via rates, see Sect. II A, and IBS through classical propagation, see Sect. II B.

Note that until this time, as can be seen in panel (b) of Fig. 8, almost all electrons (n_{total}) are trapped ($n_{\text{quasi-free}}$) inside the cluster due to their low kinetic energy. They start to leave the cluster with the onset of the IBS heating. This disagrees with the common interpretation that, when the photon frequency is larger than the first atomic ionization potential, all cluster atoms are singly ionized by one-photon absorption. Rather, the space charge built up even in a relatively small cluster such as Ar_{147} allows the electrons to become *quasi-free* only. Hence, the “ionization into the cluster”, as described in Sect. III, starts very early in the pulse. These electrons thermalize very quickly and obey a Maxwell-Boltzmann velocity distribution with a temperature T which is shown as function of time in Fig. 8c.

Figure 8b also shows the average number of localized electrons, as they have been introduced in Sect. II C. They reach a maximum ($t \approx 90$ fs) when the photo-ionization becomes unlikely. The increase of the temperature of the electron plasma (see Fig. 8c) from this point on favors a decrease of the number of localized electrons. At the point ($t \approx 120$ fs) where the cluster expansion (see Fig. 8d) starts, the temperature of the electrons plasma decreases, despite of the continuing energy absorption and the localization increases again to an average of two electrons per atom.

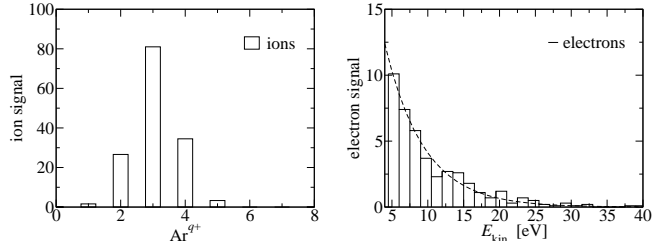


FIG. 9: The ion charge distribution (left panel) and the kinetic energy distribution of the released electrons after the cluster explosion for the same pulse as in Fig. 8. The propagation time was $t = 6.4$ ps. The electron signal can be exponentially fitted by $\exp(-E_{\text{kin}}/E_0)$ with $E_0 = 5.4$ eV (dashed line).

This transient complex behavior of electrons and ions in the cluster may be accessible experimentally soon using attosecond pulse probe techniques, for a proposal see [23]. For the time being, we present in Fig. 9 more conventional observables measurable in the experiment, such as the final charge distribution of ions and the kinetic-energy distribution of electrons for the dynamics of Ar_{147} . They have been obtained by propagation up to $t = 6.4$ ps, i.e., much longer than shown in Fig. 8. The dominating fragment is Ar^{3+} despite the fact that about five electrons (Fig. 8b) per atom have been photo-ionized. The kinetic-energy distribution of the electrons can be fitted with an exponential decay $\exp(-E_{\text{kin}}/E_0)$ with $E_0 = 5.4$ eV,

thus emphasizing the thermal origin of the electrons. The temperature of the plasma has similar values, see Fig. 8c.

V. SUMMARY

We have described a quantum-classical hybrid approach to follow the time-dependent dynamics of rare-gas clusters exposed to intense short laser pulses. Special attention has been paid to incorporate the screening of cluster ions by the electron plasma, formed by quasi-free electrons which have been ionized from their mother ions but cannot leave the cluster as a whole due

to the strong background charge. The mean time scale of these localized quasi-free electrons is determined and provides the link between the microscopic dynamics of all charged particles and the quantum dynamics of photoionization which is described by ionization rates adopted to the screening in the cluster environment.

Hence, this approach is especially well suited to tackle interaction of clusters with light from VUV and X-FEL laser sources. As an illustrative example we have discussed the dynamics of Ar_{147} exposed to a 100 fs laser pulse of $I = 7 \times 10^{13} \text{ W/cm}^2$ intensity and $\hbar\omega = 20 \text{ eV}$ photon energy.

-
- [1] J. Zweiback, R. A. Smith, T. E. Cowan, G. Hays, K. B. Wharton, V. P. Yanovsky, and T. Ditmire, *Phys. Rev. Lett.* **84**, 2634 (2000).
 - [2] H. Wabnitz et al., *Nature* **420**, 482 (2002).
 - [3] R. Santra and C. H. Greene, *Phys. Rev. Lett.* **91**, 233401 (2003).
 - [4] Ch. Siedschlag and J. M. Rost, *Phys. Rev. Lett.* **93**, 043402 (2004).
 - [5] C. Jungreuthmayer, L. Ramunno, J. Zanghellini, and T. Brabec, *J. Phys. B.* **38**, 3029 (2005).
 - [6] Z. B. Walters, R. Santra, and C. H. Greene, *Phys. Rev. A* **74**, 043204 (2006).
 - [7] U. Saalman, Ch. Siedschlag, and J. M. Rost, *J. Phys. B* **39**, R39 (2006).
 - [8] C. Deiss, N. Rohringer, J. Burgdörfer, E. Lamour, Ch. Prigent, J.-P. Rozet, and D. Vernhet, *Phys. Rev. Lett.* **96**, 013203 (2006).
 - [9] K. Ishikawa and T. Blenski, *Phys. Rev. A* **62**, 063204 (2000).
 - [10] I. Last and J. Jortner, *Phys. Rev. A* **62**, 013201 (2000).
 - [11] R. Neutze, R. Wouts, D. van der Spoel, E. Weckert, and J. Hajdu, *Nature* **406**, 752 (2000).
 - [12] Ch. Siedschlag and J. M. Rost, *Phys. Rev. Lett.* **89**, 173401 (2002).
 - [13] U. Saalman and J. M. Rost, *Phys. Rev. Lett.* **89**, 143401 (2002); *Phys. Rev. Lett.* **91**, 223401 (2003).
 - [14] C. Jungreuthmayer, M. Geissler, J. Zanghellini, and T. Brabec, *Phys. Rev. Lett.* **92**, 133401 (2004).
 - [15] Z. Jurek, G. Faigel, and M. Tegze, *Eur. Phys. J. D* **29**, 217 (2004).
 - [16] S. V. Fomichev, D. F. Zaretsky, D. Bauer, and W. Becker, *Phys. Rev. A* **71**, 013201 (2005).
 - [17] R. D. Cowan, *The Theory of Atomic Structure and Spectra*. University of California Press, Berkeley, CA 1981. See also: <ftp://aphysics.lanl.gov/pub/cowan>
 - [18] W. F. Chan, G. Cooper, X. Guo, G. R. Burton, and C. E. Brion, *Phys. Rev. A* **46**, 149 (1992).
 - [19] J. M. Rost, *J. Phys. B* **28**, L601 (1995).
 - [20] Y. B. Zel'dovich and P. Raizer, *Physics of shock waves and high-temperature hydrodynamic phenomena (vol. 1)*, p. 299, Academic Press 1966.
 - [21] H. Friedrich, *Theoretical Atomic Physics*, 3rd edition, Sect. 3.2.3, Springer Heidelberg 1998.
 - [22] B. H. Bransden and C. J. Joachain, *Physics of Atoms and Molecules*. Benjamin Cummings 2003.
 - [23] I. Georgescu, U. Saalman, and J. M. Rost, <http://arxiv.org/abs/0705.3389> (2007).